International Journal of Biological Macromolecules 276 (2024) 133793

Contents lists available at ScienceDirect

International Journal of Biological Macromolecules

journal homepage: www.elsevier.com/locate/ijbiomac

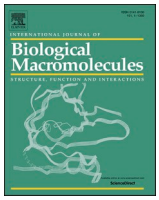

The interplay between hyaluronic acid and stem cell secretome boosts pulmonary differentiation in 3D biomimetic microenvironments

Francesca Della Sala [a], Gennaro Longobardo [a,b], Mario di Gennaro [a], Francesco Messina [c], Assunta Borzacchiello [a,*]

[a] Institute of Polymers, Composites and Biomaterials, National Research Council (IPCB-CNR), Viale J.F. Kennedy 54, 80125 Naples, Italy
[b] Department of Chemical, Materials and Production Engineering, University of Naples Federico II, Piazzale V. Tecchio 80, 80125 Naples, Italy
[c] Ospedale Evangelico Betania, Via Argine, 604, 80147 Naples, Italy

ARTICLE INFO

Keywords:
Hyaluronic acid
Secretome
Interaction

ABSTRACT

Mesenchymal stem cells (MCSs) secretome provide MSC-like therapeutic effects in preclinical models of lung injury, circumventing safety concerns with the use of live cells. Secretome consists of Extracellular Vesicles (EVs), including populations of nano- to micro-sized particles (exosomes and microvesicles) delimited by a phospholipidic bilayer. However, its poor stability and bioavailability severely limit its application. The role of Hyaluronic acid (HA) as potential carrier in biomedical applications has been widely demonstrated. Here, we investigated the interplay between HA and MSCs- secretome blends and their ability to exert a bioactive effect on pulmonary differentiation in a 3D microenvironment mimicking lung niche. To this aim, the physical-chemical properties of HA/Secre blends have been characterized at low, medium and high HA Molecular Weights (MWs), by means of SEM/TEM, DLS, confocal microscopy and FTIR. Collectively physical-chemical properties highlight the interplay between the HA and the EVs. In 3D matrices, HA/Secre blends showed to promote differentiation in pulmonary lineage, improved as the MW of the HA in the blends decreased. Finally, HA/Secre blends' ability to cross an artificial mucus has been demonstrated. Overall, this work provides new insights for the development of future devices for the therapy of respiratory diseases that are still unmet.

1. Introduction

Lung diseases are major causes of morbidity and mortality affecting millions of people around the world, with a prevalence still increasing [1–3]. Existing approaches for lung diseases focus only on reducing symptom severity and improving quality of life, but there is still an urgent unmet need for new treatments, as no current therapy has been shown to stop disease progression, restore lung damage, reverse alveolar loss, or allow complete recovery of pulmonary and systemic function [4]. In this frame, regenerative medicine can act as a new paradigm for the development and application of innovative treatments for lung diseases, that can provide both therapeutic and regenerative effects. Because of their known regenerative potential, plenty of preclinical studies have provided consistent proof of MSC based therapy effectiveness in treating many lung disorders [5] even if their bench side application is still limited to their potential tumorigenesis and handling problems.

Due to MSCs mode-of-action being mainly attributed to paracrine mechanisms, MSC derivatives, known as MSC-secretome, have also been used as alternative approaches for lung regenerative medicine. The secretome, released by MSCs in response to environmental changes and stress signals from injured tissues, consists of a myriad of bioactive soluble factors directly secreted or packaged in self-produced cargos like extracellular vesicles (EVs). EVs comprise populations of exosomes and microvesicles (MVs) that are nano- to micro-sized particles delimited by a phospholipidic bilayer, able to regulate intercellular communication and transport bioactive molecules [6,7]. These are able to regulate lineage differentiation of MSCs into different cell lines to enhance angiogenic, anti-inflammatory, anti-fibrotic and immune modulation functions [8]. Current data suggest that the MSCs-secretome can effectively mimic the therapeutic effects of MSCs in preclinical models of lung injury, circumventing many of the safety concerns associated with the use of live cells. Indeed, unlike cells, Secretomes are not able to proliferate or reprogram after administration, decreasing the risk of tumorigenicity. Additionally, the secretome can be safely stored for a long time without risking functional loss [9]. However, the direct

* Corresponding author.
E-mail address: bassunta@unina.it (A. Borzacchiello).

https://doi.org/10.1016/j.ijbiomac.2024.133793
Received 23 February 2024; Received in revised form 4 July 2024; Accepted 8 July 2024
Available online 9 July 2024

injection of MSC-secretomes has been shown to create secretome instability in vivo, as the secretome might be destroyed by enzymes or leak into adjacent tissues [10]. Thus, the possibility of combining it with biomaterials makes MSC-Secretome-based therapy a more translational strategy, potentially improvable to achieve future clinical applications. It has been proven that Secretome embedded in scaffold based on dextran sulfate-ECM hybrid material can augment pro-angiogenic factors [11]. Moreover, alginate microcapsules loaded with processed conditioned media reduce the infiltration and/or expression of CD68+ macrophages [12].

In this scenario, the use of Hyaluronic acid (HA) as a delivery system for EVs could improve the low half-life of EVs, acting as a shield and avoiding their rapid clearance, and increase stability and retention following in vivo administration. Furthermore, considering the future challenges that remain for EV clinical translation, specifically in the application of lung regeneration, HA solutions can be easily optimized in terms of viscosities [13] to accomplish the typical pulmonary administrations such as intratreacheal and inhalation routes. HA, a constituent of the lung extracellular matrix (ECM), is a polysaccharide containing repeating disaccharide units of β-1,4-d-glucuronic acid (GlcUA) and β-1,3-*N*-acetyl-d-glucosamine (GlcNAc) bound with β-glycosidic linkages [14]. It is a non-sulfate, non-immunogenic, biodegradable and biocompatible anionic glycosaminoglycan ubiquitously distributed all over the body, in connective tissue, synovial fluid, organs, and in ECM as well as in the lung parenchyma. Our previous studies demonstrated that HA enhanced the expression of the pulmonary surfactant proteins, improving the differentiation of MSCs in alveolar Type II (ATII) cells [15,16]. Furthermore, we preliminary demonstrated a synergistic effect of HA and secretome mixture in supporting cellular viability and inducing pulmonary regeneration on 2D MSC cell culture systems [17]. However, the absence of an environment in 2D culture system may provide misleading results regarding the cellular response, which often do not coincide with 3D environments in which the cells physiologically exist [18]. Indeed, in vivo stem cells are hosted in a local tissue microenvironment or niche, which comprises cells and ECM, and their crosstalk influences cell behaviors [19].

In this frame, the aim of this study was to investigate the interplay between HA and MSCs- secretome blends and their ability to promote stem cell differentiation in mature Type II Pneumocytes embedded in a 3D microenvironment mimicking pulmonary niche systems, constituted by lung ECM components. To this aim, we evaluated the chemical and physical properties of HA and MSCs-secretome blends as a function of HA Molecular Weight (MW). Since the MW of HA has an influence on both its biological functions and its physicochemical properties, low, medium and high MW HA were investigated as representative of different behaviors. Indeed, HA, depending on its MW, can form entangled molecular networks through steric interactions and self-association between and within individual chains. Moreover, the HA chains, depending on their length, are capable of binding the cellular membrane by means of hyaladherins such as CD44, hyalectans, TSG-6, RHAMM, HABP1 and HABP2, which are involved in different roles such as cell adhesion, structural support of the ECM and cell signaling. For these reasons, in solution, a physical-chemical interaction between the polysaccharide chains of the HA, depending on its MWs, and the EVs can be supposed.

In this context, a preliminary study on the behaviour of different HA MWs in solution has been performed by rheological tests, since polymers in solutions have different concentration regimes depending on their MW and this can influence the interaction. The physical-chemical interaction of the HA/Secre blends has been evaluated qualitatively by scanning and transmission electron microscopy (SEM and TEM) and by confocal microscopy. A physical-chemical characterization was performed by Dynamic Light Scattering (DLS) and Fourier-Transformed Infrared (FT-IR) analysis. Then the biological characterization, including the differentiation of MSCs into alveolar type II (ATII) cells capable of pulmonary surfactant protein production and their viability over long time was evaluated. Moreover, fluorescence recovery after photobleaching (FRAP) analysis has been used to assess the interaction of HA chains at different MWs and MVs. Finally, the penetration of the HA/Secre blends into healthy and diseased artificial mucus in an in vitro model has been studied. To the best of our knowledge, no study on the interaction of the HA/Secre blend has been reported. The data obtained in this study pave the way for the use of the HA/Secre complex for lung regeneration.

2. Material and methods

2.1. Materials

Hyaluronic acid (HA) with a weight-average molecular weight (MW) of Low (L) 200, Medium (M) 500 and High (H) 1435 kDa were kindly provided by Altergon Italia s.r.l.. Phosphate buffer saline (PBS) tablets without calcium and magnesium were obtained from MP Biomedicals Inc.. Human Umbilical Cord MSCs (hUCMSCs) were extracted from the Wharton jelly of the umbilical cord kindly gifted by Ospedale Evangelico Betania (Naples, Italy). Lysosecretome, derived from human adipose MSCs, was purchased by Pharma Exceed S.r.l.. SAGM (Lonza C-41 24) and Fetal Bovine Serum (FBS) were purchased from Lonza (Basel, Switzerland). Eagle's Minimum Essential Medium (EMEM), Hyclone, (USA). Penicillin, streptomycin (10,000 U/ml) from Invitrogen and Life Technologies (Carlsbad, CA) were employed. Trypsin and Ethylenediaminetetraacetic acid (EDTA) were from HiMedia (Mumbai, India). Formalin, bovine serum albumin (BSA) and 4′,6-diamidino-2-phenylindole (DAPI) were purchased from Sigma-Aldrich (USA). SPC rabbit antibody from Abcam. Fitch-conjugated anti-rabbit antibody (Millipore, Billerica, MA, USA). Human pulmonary surfactant associated protein (SP) SPA, SPB, SPC and D ELISA kits were obtained from Elabscience.

2.2. HA solutions rheological characterization

In order to preliminarily study the behaviour of different MW HA chains in solution, rheological tests were performed by means of a MARS rheometer™ III (TermoFisher Scientific, Waltham, MA, USA). The geometry used was Cone C60/1°CS L. Flow curves were conducted at 25 °C on LMWHA, MMWHA and HMWHA solutions at different concentration ranges (0.125–40 mg/ml, 0.125–30 mg/ml and 0.125–11 mg/ml, respectively) in distilled water. The range of shear stresses varied from 0.01 to 1100 s^{-1} depending on polymer MW and concentration to obtain a curve representative of their behaviour. Each flow curve was repeated in triplicate and error-correlated data were fitted on OriginPro 2018 software. *Ellis-fluid model* was implemented to study the dependency of viscosity on the shear rate calculated with Eq. (1):

$$\eta(\dot{\gamma}) = \frac{\eta_0}{1 + (\lambda\dot{\gamma})^{1-n}} \tag{1}$$

where η_0 stands for the *zero-shear* viscosity, λ is a characteristic time constant representing the relaxation time of the polymer solution, and n is a flux index. Then the fitted values for zero-shear viscosity (accompanied by the fit uncertainties) were used to calculate the specific viscosities (Eq. (2)):

$$\eta_{sp} = \frac{\eta_0 - \eta_s}{\eta_s} \tag{2}$$

where η_s is the *solvent viscosity* (water). Then, the specific viscosities have been plotted on a log-log graph as a function of concentration for all MWs and three weighted linear fits for each of these plots were performed. In order to understand the critical concentrations for polymer coils overlapping, these have been reported as a function of MW to obtain a phase-diagram useful for highlighting HA solution regimes at different MWs (Fig. S1A).

2.3. HA/ secretome blends preparation

By rheological results, we selected HA concentration among the dilute regime (0.05 %, 0.025 % and 0.02 % LMW, MMW and HMW, respectively) and the semidilute unentangled regime (0.5 %, 0.25 %, and 0.1 %, for LMW, MMW and HMW, respectively). Secretome has been used in all experimental sets at a concentration of 0.2 mg/ml ($2*10^4$ human adipose MSCs equivalent) blended in the HA (LMW, MMW and HMW) solutions. As regards the cell viability test, HA was dissolved in DMEM and stirred for 3 h in order to guarantee the homogeneity of the solution. To carry out the differentiation experiments, a suitable amount of HA was dissolved in an appropriate volume of SAGM and then kept under stirring for 3 h. The solutions obtained from the previous procedure were sterilized by filtration using 0.22-μm filters.

2.4. SEM and TEM microscopy

Morphological evaluation of HA/secretome blends has been investigated by scanning electron microscopy (SEM, Quanta 200 FEG, FEI Company, Hillsboro, OR, USA) and transmission electron microscopy (TEM, FEI Tecnai G12 Spirit Twin, Eindhoven, The Netherlands). For SEM analysis, Secre and Secre/HA blends were prepared at the above-mentioned concentrations. Then, samples were freeze-dried and Au/Pd -sputtered to perform the analysis at a beam voltage varying from 20 to 5 kV. For TEM, LaB6 emission sources (120 kV, spot size 1) using 400 mesh carbon-coated copper grids were used at room temperature (RT). The carbon-coated copper grid was immersed in Nile red-treated (see paragraph 2.5) Secre or HA/Secre blends and, after the drying step, the grid was placed on a rod holder for TEM characterization, acquiring a minimum of four micrographs per grid.

2.5. Dimensional distribution and zeta potential

Intensity-average hydrodynamic radius and ξ potentials of the samples have been determined by means of DLS measurements with a Zetasizer Nano (Malvern Instruments, Malvern, UK). For size and zeta size measurements, Secre (0.2 mg/ml) was suspended in ultrapure water or HA solutions in dilute condition (0.1 % LMWHA, 0.05 % MMWHA and HMWHA).

2.6. Fourier-transformed infrared (FT-IR) analysis

HA/ Secre blends at different HA MW, LMWHA, MMWHA, HMWHA and Secretome were obtained and characterized using Perkin Elmer Frontier Fourier Transform Infrared Spectroscopy FT-IR (Waltham, MA, USA), with a single-reflection, universal ATR-IR accessory. All spectra were recorded between 4000 and 650 cm^{-1} with a resolution of 4 cm^{-1}.

2.7. Nile red/Alcian blue staining and confocal microscopy analysis

In order to qualitatively observe the interaction between HA/ Secretome bioactive materials, confocal microscopy was performed. First, secretome EVs were stained with Nile-red, which is used to detect intracellular lipid droplets [20]. Briefly, Nile-red solubilized in acetone (1 mg/ml) was diluted 1000× in distilled water and incubated in distilled water with lyophilized secretome (1 mg/ml) at 37 °C for 60 min. Then, HA chains were stained with Alcian Blue, glacial acetic acid (30 % *v*/v) and ethanol (70 % v/v) at pH ~2 were added to Alcian Blue (1 % *w/v*). This solution was added (1:100) to HA solutions at different MWs and stirred for 30–40 min at RT. Then Nile red-stained secretome solutions, to a final 100× concentration, were suspended in the Alcian Blu HA solutions, and stirred for 30 min at RT. Then, the samples were observed by confocal microscope system (Leica TCS SP8) with a 63× oil immersion objective. Excitation lasers were set to work at 515 nm for Nile red and 480 nm for Alcian Blue; while emission detection ranges were set in the interval 620–720 nm for Nile red and 464–486 nm for Alcian Blue. Images were acquired with a resolution of 1024 × 1024 pixels by z-stacking, and the thickness of each z-slice was set equal to 0.1 μm.

2.8. Biological properties

2.8.1. Cell culture

The hUCMSCs, at early passages (1–6), were grown in a T-75 cell culture flask (VWR, Radnor, PA, USA) in complete DMEM, supplemented with 10 % FBS and antibiotics (penicillin G sodium 100 U/ml, streptomycin 100 U/ml), in a humidified and controlled atmosphere at 37 °C and 5 % CO_2, changing medium every 3–4 days. The cells were detached, after confluent growth was reached, with a 0.25 % trypsin - EDTA solution and washed twice with PBS. The resulting cell suspensions were centrifuged (5 min, 1000 rpm; BRK55/10 Centrifuge by Centurion Scientific Ltd., UK), the supernatant separated, and the cells re-suspended in fresh culture medium. Viable cells were counted using the TC20 automated Cell Counter (Biorad, USA).

2.8.2. Gel mimicking 3D microenvironments systems preparation

In order to investigate the influence of the HA/Secre blends on pulmonary differentiation in 3D biomimetic microenvironments, the hUCMSCs have been cultured in a 3D gel based on COLL and HA, which are the main constituents of the ECM pulmonary niche [21]. The COLL gels, used as control, were prepared by diluting COLL stock solutions at an initial concentration of 2.4 mg/ml with 10× PBS (8:1 volume ratio). To obtain COLL fibrillogenesis, the pH was adjusted to 7.4 ± 0.2 by dropwise addition of NaOH and/or HCl. The 3D microenvironments based on HA/COLL hydrogels were obtained by promoting COLL fibrillogenesis in the presence of the different HA MWs. HA powder was previously sterilized by means of exposition to UV irradiation and then mixed with the COLL solution. To allow the gelification, the procedure described above was used. The HA/COLL gels were prepared using LMW, MMW and HMW HA, 0.5 %, 0.25 %, and 0.1 % *w/v*, respectively, corresponding to a HA:COLL weight ratio of 2.7:1, 1.4:1 and 0.5:1, respectively. The samples were named LMWHA/COLL, MMWHA/COLL and HMWHA/COLL [16]. Then, to obtain the 3D mimicking environment systems with embedded hUCMSCs, the cells were dispersed in COLL and HA/COLL solutions respectively, transferred in appropriate cell culture dishes, depending on the type of experiment, and incubated at 37 °C for 1 h to allow COLL fibrillation. After, fresh cell culture medium was added to the top of the gels.

2.8.3. Immunofluorescence anti-SPC

In order to assess the differentiation of the hUCMSCs in ATII cells, the qualitative expression of Surfactant Protein C (SPC) has been evaluated by immunofluorescence against the SPC antibody. hUCMSCs were cultured for 21 days and seeded on fluorodish −35 mm (World Precision Instruments, Inc.), fixed in 10 % Formalin for 3 h, permeabilized with 0.1 % Triton X-100, blocked with 1 % BSA and incubated with SPC rabbit antibody (Abcam) diluted in 1 % BSA at 4 °C overnight. After washing with PBS three times, Fitch-conjugated anti-rabbit antibody (Millipore, Billerica, MA, USA.) was added to the cells for 3 h at room temperature. The qualitative expression of Cluster of Differentiation 73 (CD73) has been evaluated by immunofluorescence against the CD73 antibody. hUCMSCs were cultured for 21 days and seeded on fluorodish −35 mm (World Precision Instruments, Inc.), fixed in 10 % Formalin for 1 h, permeabilized with 0.2 % Tween 20 for 1 h, blocked with 1 % BSA and incubated with CD73 mouse antibody diluted in 1 % PBS/BSA at 1:100 dilutions for 2 h at 4 °C. Lastly, for all samples, cell nuclei were stained with blue DAPI (10 min at 37 °C), and observed by confocal microscope system (Leica TCS SP5 MP) with a 63× oil immersion objective. Images were acquired with a resolution of 1024 × 1024 pixels.

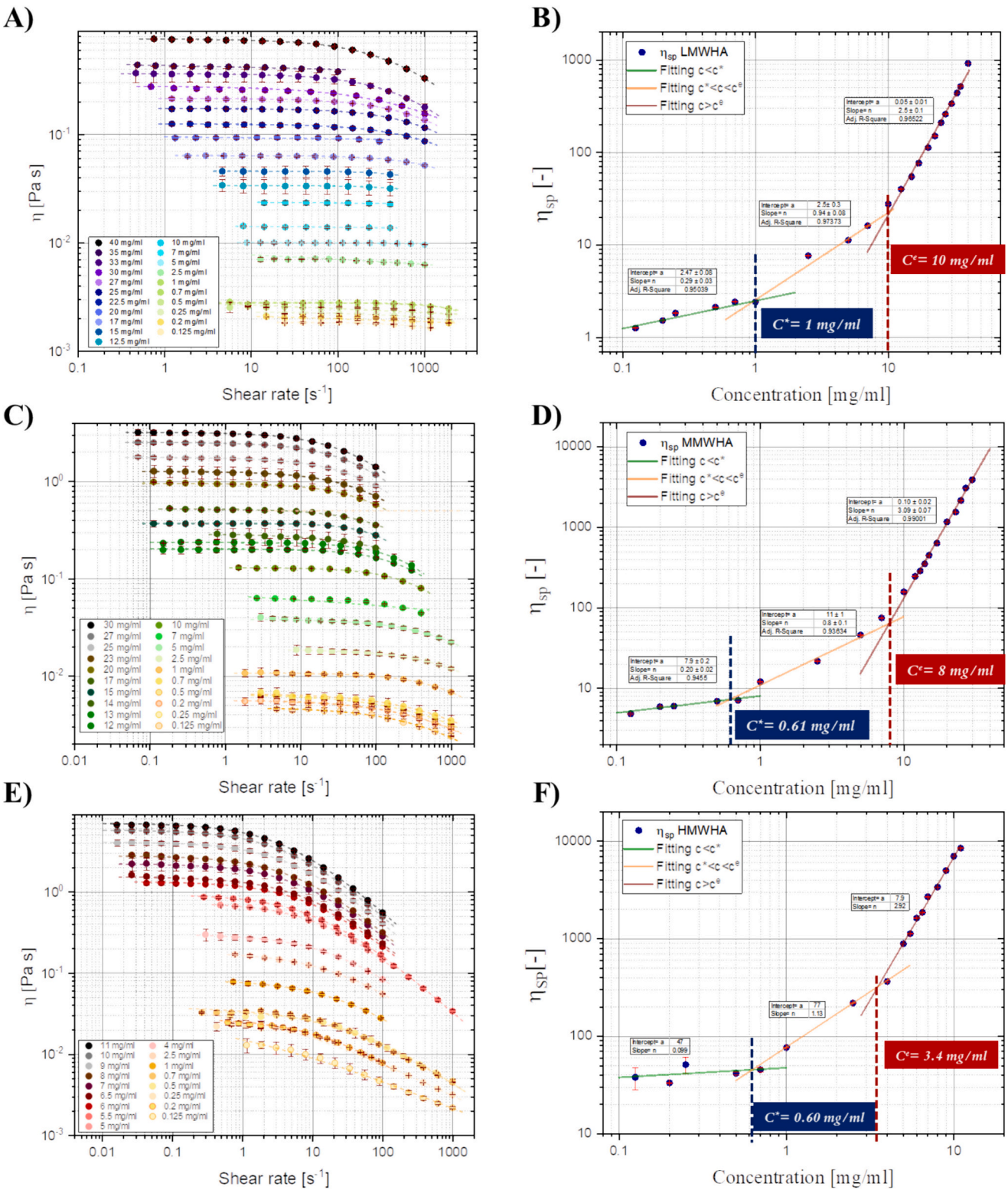

Fig. 1. Rheological characterization of HA solutions. Flow curves of LMWHA (A), MMWHA (C) and HMWHA (E) at different concentrations; experimental triplicates were fitted using the Ellis model (dashed lines). Zero shear viscosities obtained from the fit at different concentrations were used to plot specific viscosities as a function of HA concentration to obtain the critical overlap concentration C* for the onset of semidilute unentangled solution and the critical entanglement concentration C^e for LMWHA (B), MMWHA (D) and HMWHA (F).

2.8.4. Surfactant proteins expression

In order to evaluate the quantitative expression of human pulmonary SP A- B—C and D, the supernatants for analysis were collected after 21 days of exposure to the solutions, and then examined using SP A-B-C and D ELISA kits according to manufacturer protocol.

2.8.5. Cell viability

Cell viability tests were performed after 1, 7, 14 and 21 days

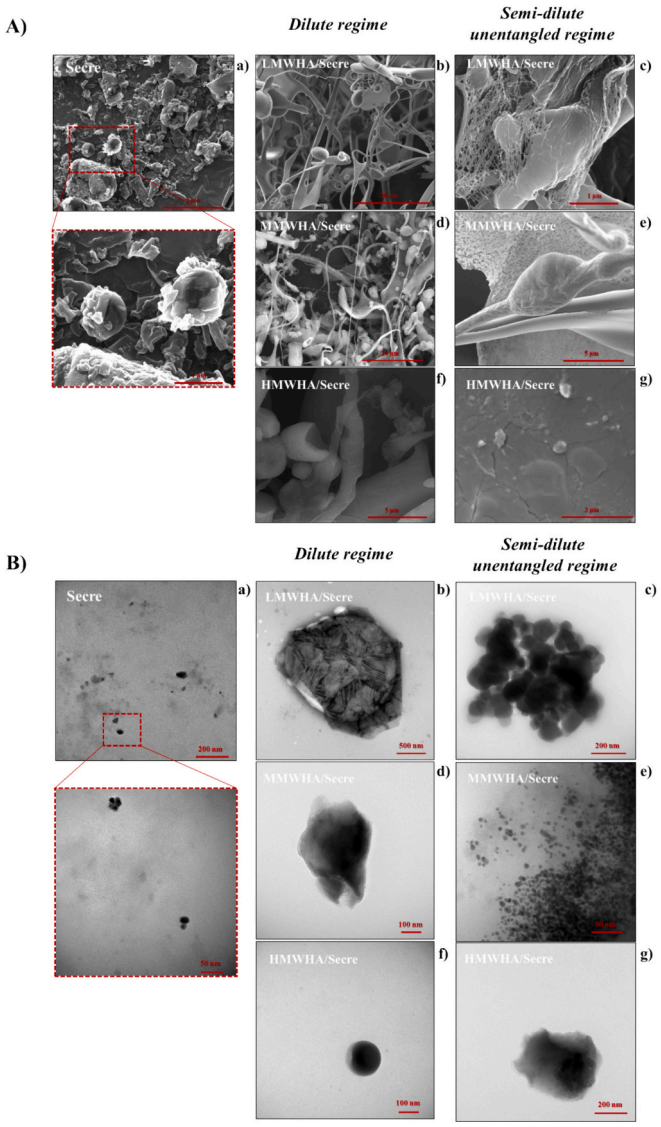

Fig. 2. Morphological analysis by electron microscopy. Representative SEM images of Secre (A.a) and HA/Secre blends in dilute (A.b, A.d and A.f) and semidilute unentangled (A.c, A.e and A.g) LMWHA, MMWHA and HMWHA regimes. Representative TEM images of Secre (B.a) and HA/Secre blends in diluted (B.b, B.d and B.f) and semidilute unentangled (B.c, B.e and B.g) LMWHA, MMWHA and HMWHA solutions.

(differentiation time). hUCMSCs were seeded at a density of 6×10^3 cells/ml embedded in COLL gels and in HA/COLL SIPNs on 96-wells (World Precision Instruments, Inc.) and exposed for 1, 7, 14 and 21 days to MEM, secretome alone, SAGM implemented with LMWHA, MMWHA and HMWHA, with and without secretome, respectively. The cells were seeded in each well in triplicate and then the Alamar blue assay (AB) was performed by adding AB reagent (10 % *v*/v) to the samples and incubating at 37 °C for 5 h. The absorbance of the samples was measured using a spectrophotometer plate reader (Multilabel Counter, 1420 Victor, Perkin Elmer) at 570 nm and 600 nm. AB is an indicator dye that incorporates an oxidation-reduction indicator that changes colour in response to the chemical reduction in the growth medium, resulting from cell viability. Cells seeded in only COLL were used as a control. Data are expressed as the percentage difference between treated and control to evaluate the percentage of reduction (Reduction %), which is calculated with the following formula (Eq. (3)):

$$Reduction\ (\%) = \frac{(O_2 \times A_1) - (O_1 \times A_2)}{(O_2 \times P_1) - (O_1 \times P_2)} \times 100 \quad (3)$$

where *O*1 is the molar extinction coefficient (*E*) of oxidized AB at 570 nm; *O*2 is the *E* of oxidized AB at 600 nm; *A*1 is the absorbance of test wells at 570 nm; *A*2 is the absorbance of test wells at 600 nm; *P*1 is the absorbance of control well at 570 nm; and *P*2 is the absorbance of control well at 600 nm. The percentage of reduction for each sample was normalized to the percentage of reduction for the control to obtain the cell viability percentage [22].

2.9. Fluorescence recovery after photobleaching (FRAP)

FRAP was performed on Nile-red stained secretome alone and in HA/Secre blends in semidilute regime in order to study their possible biological effects. Confocal microscope system (Leica TCS SP8) has been used. Images were acquired with a 63× oil-immersion objective, and a 515 nm Argon laser line was used with a ~ 95 % laser excitation pulse. A circular bleach region was selected with a diameter of ~1.5 μm. The recovery was recorded at a rate of 1.2 s/frame, 150 frames in total. Laser power was tuned to ensure that the final non-bleached background fluorescence was within 15 % of the initial non-bleached background fluorescence on average. For each sample, a minimum of three independent FRAP experiments were performed and fluorescence intensities were normalized. Data were fitted on Matlab© with an exponential recovery-like-shape curve by plotting the normalized fluorescent intensity value to times calculated in Eq. (4):

$$I_n(t) = I_\infty \left(1 - exp\left(-\frac{t}{\tau_{1/2}}\right)\right) \quad (4)$$

where I_n represents normalized fluorescence intensities, I_∞ is the normalized intensity after-recovery and $\tau_{1/2}$ represents the *halftime recovery*, the time it takes for the curve to reach 50 % of the plateau fluorescence intensity level. Then, the *mobile fraction* (M_f) % can be obtained calculated by Eq. (5):

$$M_f = \frac{I_\infty - I_0}{I_1 - I_0} x\ 100 \quad (5)$$

where I_∞ is the normalized intensity after-recovery, I_0 is the normalized averaged intensity before bleaching and I_1 is the normalized intensity after bleaching.

2.10. In vitro assessment of mucus penetration

Penetration of secretome EVs (Nile-red stain) and HA/Secre blends into an in vitro model of healthy and diseased artificial mucus (HM and DM, respectively) has been tested adapting the protocol from Wu et al. [23]. Briefly, 1 ml of gelatin 15 % (*w*/*v*) solution was placed at the bottom of multiple glass vials, storing at 4 °C until gelling. Then, 1.5 ml of HM and DM on top of the gelatin layer have been pipetted for each sample. The composition and concentrations of artificial HM and DM are reported in Table S1. Then, 1.5 ml of Nile red-stained secretome alone and in HA solutions, at semidilute concentration, was deposited on the surface of the HM and DM layers and placed at 37 °C for 5 h and 24 h to allow perfusion. Then, to ensure that samples arriving at the gelatin layer remain in that layer, the samples were cooled to 4 °C to strengthen the gelatin layer and the HM and DM on top were poured off, after the gelatin was heated, softened and stirred well. To quantify mucus penetration ability, the fluorescence intensity (FI) of different samples was analyzed by a spectrofluorometer (Multilabel Counter, 1420 Victor, PerkinElmer) at a 525–605 nm excitation wavelength. The percentage of mucus penetration was calculated, after subtracting the gelatin fluorescence, using the following Eq. (6):

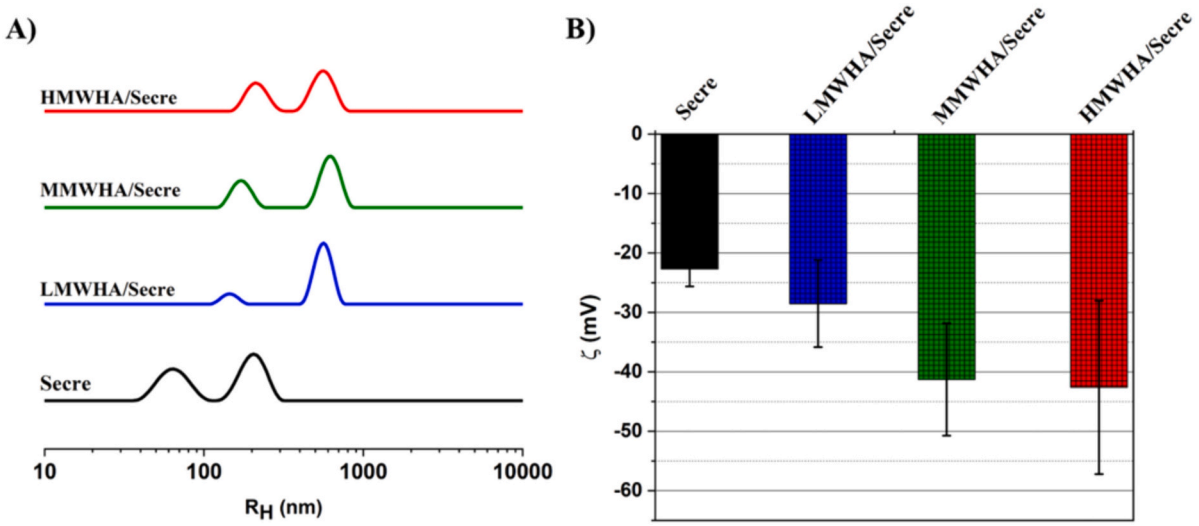

Fig. 3. Hydrodynamic size and surface charge of Secre and HA/Secre suspensions for LMWHA, MMWHA and HMWHA. Dimensional distribution of Secre and HA/Secre blends in the diluted regime (A) and zeta potential of Secre and HA/Secre blends in the diluted regime (B).

Table 1
Average hydrodynamic radius (<R_H>) and polydispersity index (PDI) of Exosomes and MVs determined by means of DLS for Secre, LMWHA/Secre, MMWHA/Secre and HMWHA/Secre solutions.

	Exosomes		MVs	
Sample	<R_H> (nm)	PDI (−)	<R_H> (nm)	PDI (−)
Secre	65.4 ± 1.4	0.04 ± 0.01	210 ± 7	0.032 ± 0.003
LMWHA/Secre	80 ± 30	0.016 ± 0.006	380 ± 60	0.016 ± 0.002
MMWHA/Secre	180 ± 40	0.028 ± 0.013	620 ± 70	0.024 ± 0.005
HMWHA/Secre	189 ± 13	0.029 ± 0.006	490 ± 50	0.05 ± 0.02

$$Mucus\ penetration\ (\%) = \frac{FI\ HA/Secre\ blend}{FI\ Secretome} \times 100 \quad (6)$$

2.11. Statistical analysis

The results were expressed as the mean ± standard deviation (SD). Data analysis was performed using Graphpad® software. The repeated results were compared with the ordinary one-way analysis of variance (ANOVA), and a P value <0.0001 was considered significant.

3. Results

3.1. HA solutions rheological characterization

Rheological tests were performed to characterize the regime concentrations of different MWs HA in solution, to have a more rational approach to the experiment design and data interpretation in the study of the interplay of HA/Secre blends. Previous studies have proved that 0.5 %, 0.25 %, and 0.1 %, for LMW, MMW and HMW HA, respectively, in combination with Secre can positively support cell viability and affect lung regeneration [17]. However, polymers in solution have different concentration regimes depending on their MW, and this can influence the interaction of another component in solution in terms of physical-chemical and biological properties [24]. Flow curves were measured on LMWHA (Fig. 1A), MMWHA (Fig. 1C) and HMWHA (Fig. 1E) at different concentrations, showing the typical shear-thinning behaviour of polymeric solutions for all samples. The viscosity dependence of the shear rate was fitted with the Ellis fluid model (Eq. (1)) to obtain the zero shear rate viscosities η_0, used to calculate the specific viscosity η_{sp} (Eq. (2)). The plots of η_{sp} against polymer concentration for LMWHA, MMWHA and HMWHA are reported in Fig. 1B, D, F, respectively. Three main linear trends with different slopes were detected, representative of a power-law dependency of η_{sp} from HA concentrations, in agreement with theoretical predictions. [25,26]. The three linear trends, fitted with a straight line in the log-log plot, represent the three concentration regimes: dilute, semidilute unentangled and semidilute entangled regimes [27].

The overlap concentration (C*), at which the semidilute unentangled regime starts, was determined by the intersection of the linear fittings of the dilute and the semidilute unentangled regimes. In the same way, the entanglement concentrations (C^e), at which the semidilute unentangled ends and the semidilute entangled regime starts, were determined by the intersection of the linear fittings of the two regimes. HA solution, in the dilute regime, can be regarded as a heterogeneous solution, assumable to be temperature-independent [26]. In fact, inside the HA coil, the polymer concentration is C*, while outside it is null. Therefore, HA/Secre blends were studied with HA in a dilute regime to evaluate the morphological and surface properties, and particularly the effect of HA on the Secre dispersion, minimizing the chain-to-chain interaction. Then, as regards higher polymer concentrations, the properties of HA/Secre blends with HA in a semidilute untangled regime were investigated, since in this condition the effect of biological response on lung regeneration has been observed [17]. And this is probably due to the ability of HA solutions in the semidilute concentration regime to act as carriers without hindering the mobility of the vesicles [28]. Conversely, in the semidilute entangled regime, the formation of an interpenetrated polymer network, as shown by frequency sweep spectra (Fig. S1C), was observed. In this state, the vesicles would be immobilized in the polymeric network with a caging effect around them, limiting their migration and hindering complex formation by the association of external receptors, yielding lower release rates within the cells [29,30].

3.2. SEM and TEM microscopy

To investigate the morphology of HA/Secre blends, SEM and TEM have been performed. SEM images of Secre, acquired as control (Fig. 2A. a) showed spherical MVs with diameters up to 1 μm and exosomes with diameters comprised between 50 and 200 nm in accordance with the manufacturer product. Images in the presence of HA were acquired at dilute and semidilute unentangled regimes for all the MWs. All the

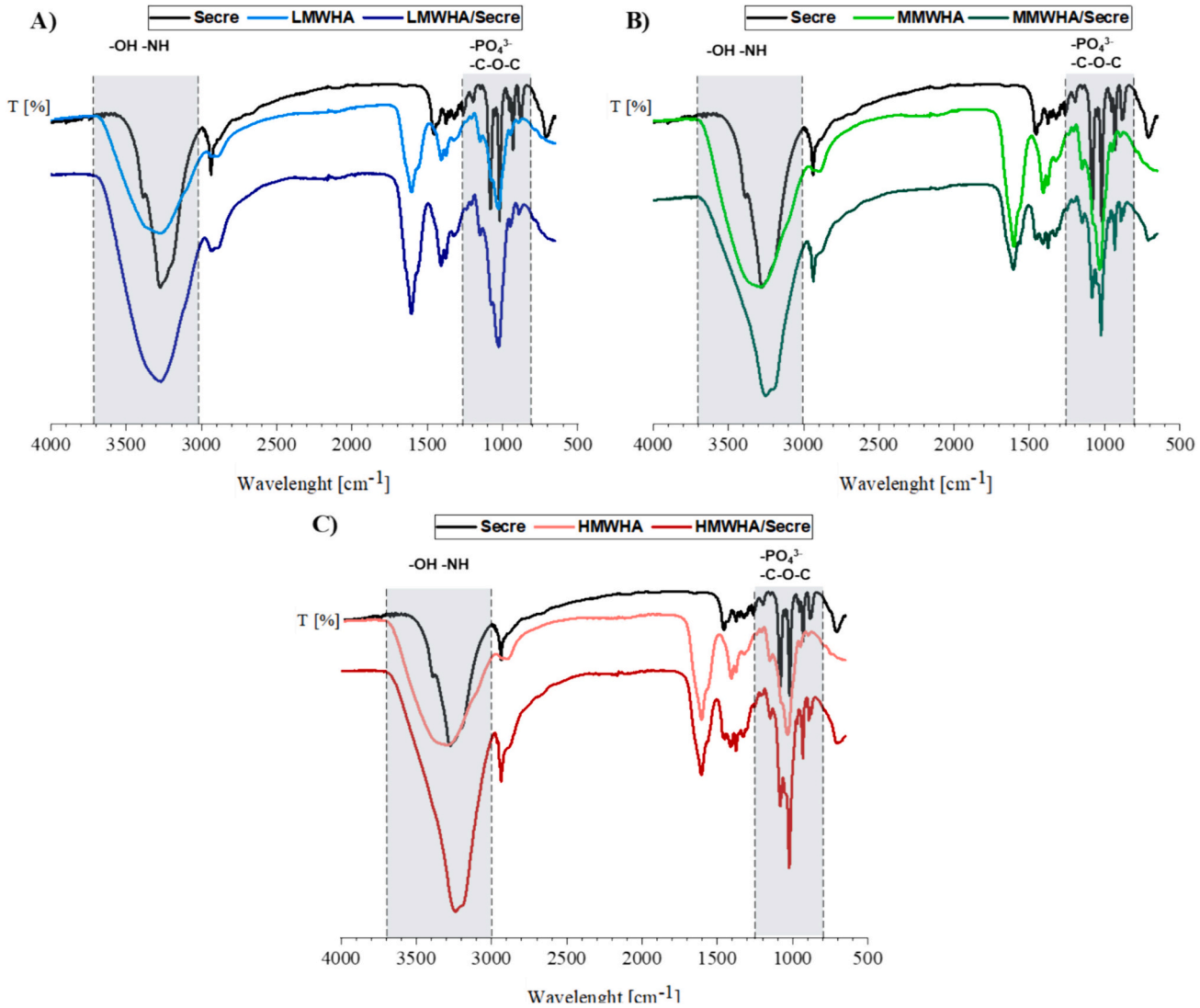

Fig. 4. ATR-FTIR spectra of Secretome, LMWHA and LMWHA/Secre (A); Secretome, MMWHA and MMWHA/Secre (B); Secretome, HMWHA and HMWHA/Secre (C). The ranges of wavelength associated with the stretching of -OH and -NH (3700–3000 nm^{-1}) and with the stretching of $-PO_4^{3-}$ and C-O-C (1265–880 nm^{-1}) are highlighted in gray, showing the peak shift and change in intensity in HA/Secre blends.

Table 2
Peak assignment for FTIR Spectra of Secre, LMWHA, MMWHA, HMWHA, LMWHA/Secre, MMWHA/Secre, and HMWHA/Secre.

	Secre	LMWHA	LMWHA/Secre	MMWHA	MMWHA/Secre	HMWHA	HMWHA/Secre
Stretching -OH -NH	3389 3276	3268	3287	3287	3256	3299	3248
Stretching -CH	2937	2886	2936 2888	2890	2936 2881	2889 2937	2879
Stretching -C=O	1655 (Amide band I)	1606	1606	1604	1605	1606	1607
Bending -NH	1549 (Amide band II)	–	–	–	1560	–	1561
Stretching -C-N		1407	1409	1408	1408	1408	1412
Bending $-CH_2$	1456	–		–	1451	–	1452
Bending $-CH_3$	1376	–	1377	–	1376	–	1377
Stretching PO_4^{3-} C-O-C	1261,1053 1019,884	–	–	–	1263,1051 1023,890	–	1263,1051 1022,891

images show a polymer matrix, whose mesh size decreases as concentration and MW increase. In the dilute regime (Fig. 2A.b, d, f), it is possible to distinguish the shapes of MVs and exosomes, which appear to be covered by the polymer. Conversely, in images acquired for semi-dilute regime systems (Fig. 2A.b, d, f), micrometric spherical objects, MVs, are embodied in the polymer matrix, while the exosomes are less

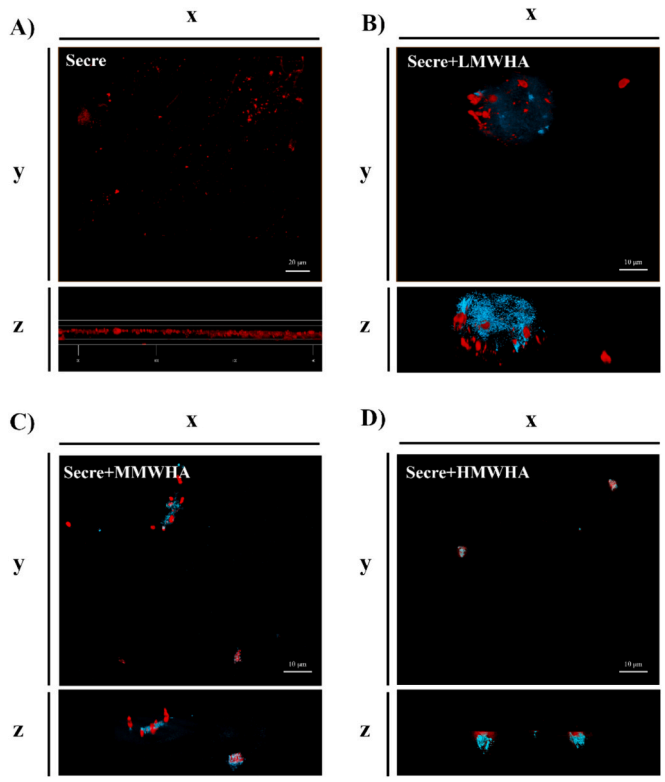

Fig. 5. Confocal microscopy of Secretome (A) and HA/Secre blends for LMWHA (B), MMWHA (C) and HMWHA (D). Secretome (Exosomes and MVs) were stained with Nile-red. Instead, HA chains were stained with Alcian Blue.

distinguishable, because they are probably incorporated in the matrix itself. The TEM images (Fig. 2B) confirmed this trend, allowing for better investigation of the behaviour of HA/Secre blends. In Fig. 2B b., d., f., it is possible to appreciate how HA tends to cover single MVs and exosomes in a dilute regime for all the MWs. While, in the semidilute unentangled regime (Fig. 2B c., e., g.), the presence of HA appears to promote the formation of a polymer layer bridging different vesicles.

3.3. Dimensional distribution and zeta potential

The size distribution and surface charge of HA/secre blends and Secre as control were analyzed by means of DLS and ξ potential measurements. Since the systems under examination intrinsically do not have monomodal size distributions, the distribution of the hydrodynamic radius (R_H) was obtained using the CONTIN algorithm to analyze the correlation data [31,32]. The Secre sample exhibited a bimodal R_H distribution, with one population in the range 30–100 nm, due to the presence of exosomes, and one population in the range 100–300 nm, due to the presence of MVs [33]. In the same way, the HA/Secre samples also exhibited a bimodal R_H distribution. A representative R_H profile for each sample was reported in Fig. 3A, and the results of DLS analysis, in terms of average hydrodynamic radius $< R_H >$ and polydispersity index (PDI), were reported in Table 1.

It is possible to observe how for all the HA/Secre samples the $<R_H>$ resulted higher both for exosomes and for MVs: the exosome $<R_H>$ raised from 65.4 nm to 80 nm for LMWHA/Secre, 180 nm for MMWHA/Secre and 189 nm for HMWHA/Secre. In the same way, the $<R_H>$ of the second population associated with MVs rose from 210 nm for Secre to 320 nm for LMWHA/Secre, 620 nm for MMWHA/Secre, and 490 nm for HMWHA/Secre. These results are probably due to the covering of EVs by HA, as shown by microscopy images. As regards the non-linear progression of the size, it might be due to differences in packing of macromolecules around the EVs because of the difference in size of HA at different MWs [34]. In this sense, differences in the way HA covers EVs can be observed from the results reported in Fig. 3B, in which the ξ potential of Secre (−23 mV) became more negative from LMWHA/Secre (−28 mV) to MMWHA/Secre (−41 mV) and HMWHA/Secre (−42 mV). These data suggest that LMWHA forms a less homogeneous shell around Secre EVs compared to MMWHA and HMWHA.

3.4. Fourier-transformed infrared (FT-IR) analysis

The HA/Secre blends interaction has been investigated by FTIR (Fig. 4). FTIR spectra show the single components of the LMWHA, MMWHA, HMWHA, and the Secretome alone compared to the LMWHA/Secre (A), MMWHA/Secre (B) and HMWHA/Secre (C) blends. The results of the peak analysis are reported in Table 2. Secretome spectra show, in accordance with the literature [20], bands at around 1457 cm^{-1} and 1377 cm^{-1} related to CH_2 and CH_3 groups of alkyl chains. The signals at 1655 cm^{-1} and 1549 cm^{-1} are the C═O stretching and N—H bending peaks, typical of polypeptides, that are commonly referred to as the amide I and amide II bands, respectively, confirmed the presence of lipid and protein [35]. The bands detected in the spectral region between 1260 and 880 cm^{-1} are due to the stretching vibrations of the phosphodiester groups (PO_4^{3-}) of phospholipids and to the C-O-C stretching vibrations of phospholipids, triglycerides and cholesterol esters. In the HA spectra for each MW, it is possible to identify the typical signals of the –OH and –NH stretching in the region between 3000 cm^{-1}–3700 cm^{-1}, due to the hydroxyl and N-Acetyl groups on the backbone of the polymer. The peaks in the region between 3000 cm^{-1} and 2700 cm^{-1} are associated with the stretching of $–CH_2$ and $–CH_3$, while the peaks at 1600 cm^{-1} and 1412 cm^{-1} are associated with the symmetric and asymmetric stretching of –COO groups. Finally, at 1030 cm^{-1} the C-O-C symmetric stretching ether bands are observed. The comparison between the spectra of the HA/Secre blends with the single components provided information about the interaction that occurred in the blends. In the MMWHA/Secre and HMWHA/Secre spectra, the characteristic signals of both components were observed, suggesting the presence of both of them in the lyophilized powder. Furthermore, shifts in maximum absorption wavenumber were observed for the –OH and –NH absorption bands, which are present for both HA and Secre, and for the signals between 1261 cm^{-1} and 884 cm^{-1}, that are associated with the vibrating modes of groups in the hydrophilic moiety of the lipids of the EVs. At the same time, no shifts were observed in the signals associated with the hydrophobic internal moiety of the EVs. These data suggest that, if an interaction between HA and Secre does occur, it implicates the external hydrophilic heads of phospholipids. Indeed, the shift and change in intensity involve hydrogen bond acceptor groups (-PO_4^{3-} and C-O-C) [36], present in phospholipids, and hydrogen bond donor groups (-OH and -NH) [37] present on the HA backbone. Thus, a possible hypothesis of interplay could be related to the establishment of intermolecular hydrogen bonds between the hydrophilic heads of phospholipids and HA chains. In the case of LMWHA/Secre blends, the presence of Secre is suggested by the maximum at 3287 cm^{-1} (-OH stretching band) and at 2936 cm^{-1} (-CH stretching peak). This is probably because the HA/Secre mass ratio, held constant as for the other experiments, was too high to detect all the IR absorption peaks of Secre. Indeed, in this case, the EVs are embedded in a dense polymer matrix of LMWHA, as also suggested by the electron microscopy images.

3.5. Confocal microscopy analysis

In order to further investigate the arrangement of the HA around Secre in the blends, the confocal microscopy technique has been used (Fig. 5). In particular, Fig. 5A shows Secretome Nile red-stained, as well as their wide dimensional distribution. Then, the addition of HA, stained by means of Alcian Blue, shows a cloud of HA chains (Blue) around the components of MVs and exosomes (Red) (Fig. 5B, C, D). More specifically, the LMWHA and MMWHA would seem to group the components

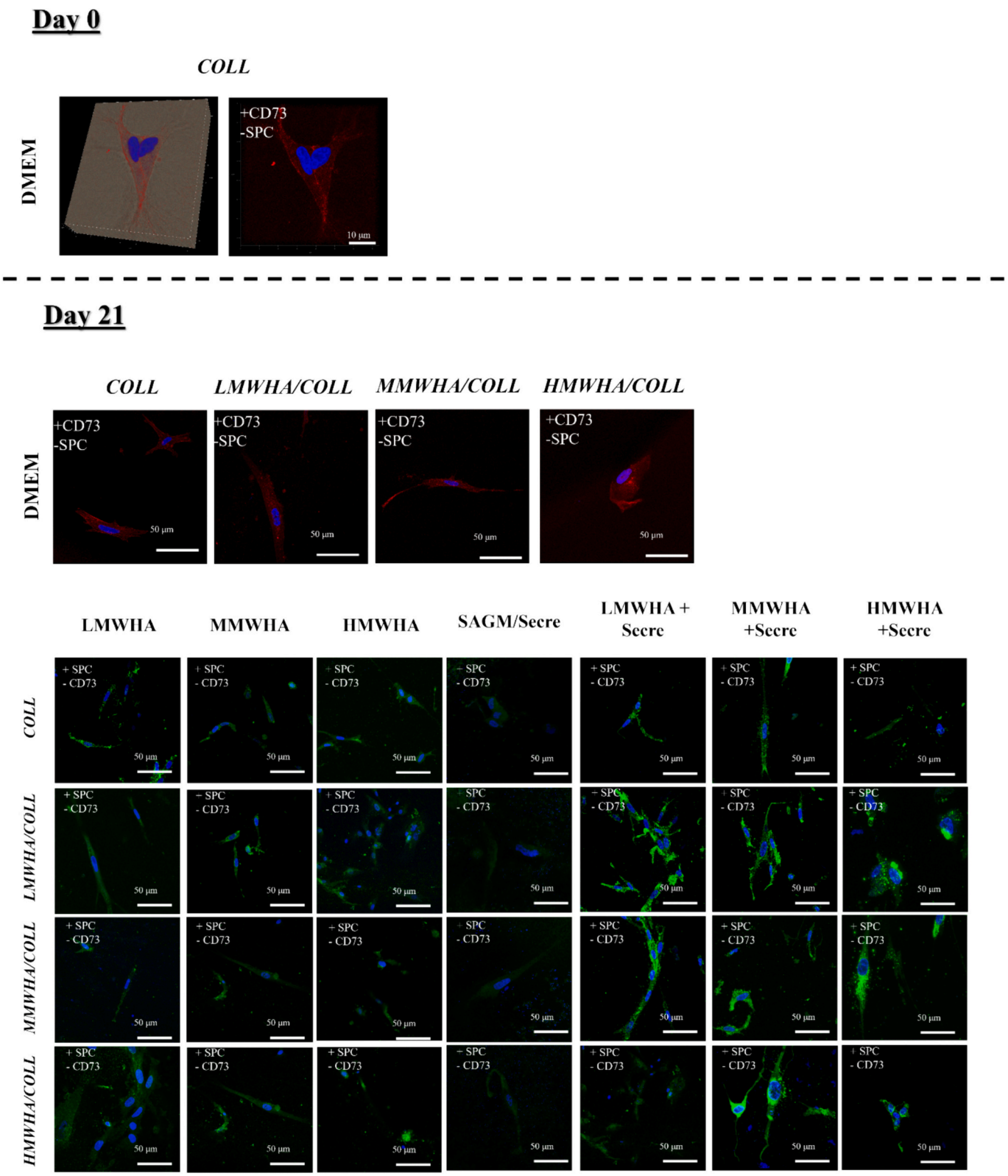

Fig. 6. Representative confocal images of immunoreactive SPC cells and CD73 stemness marker expression by immunofluorescence in a 3D biomimetic lung niche composed of COLL or COLL/HA gels at different MWs. Images were obtained after the incubation of Secre, HA solutions and HA/Secre blends implementing SAGM at day 0 and after 21 days of incubation. Nuclei were stained with blue DAPI. On Day 0 or Day 21 of DMEM culturing, positive expression of CD73 (red) indicates the presence of undifferentiated stem cells. Positive expression of SPC (green) in the cytoplasm was assessed after 21 days of exposure with implemented cell-media, indicating the qualitative expression of differentiated ATII cells compared with the untreated control (CTR DMEM). Scale bar: 10 µm for COLL at Day 0 and 50 µm for other images.

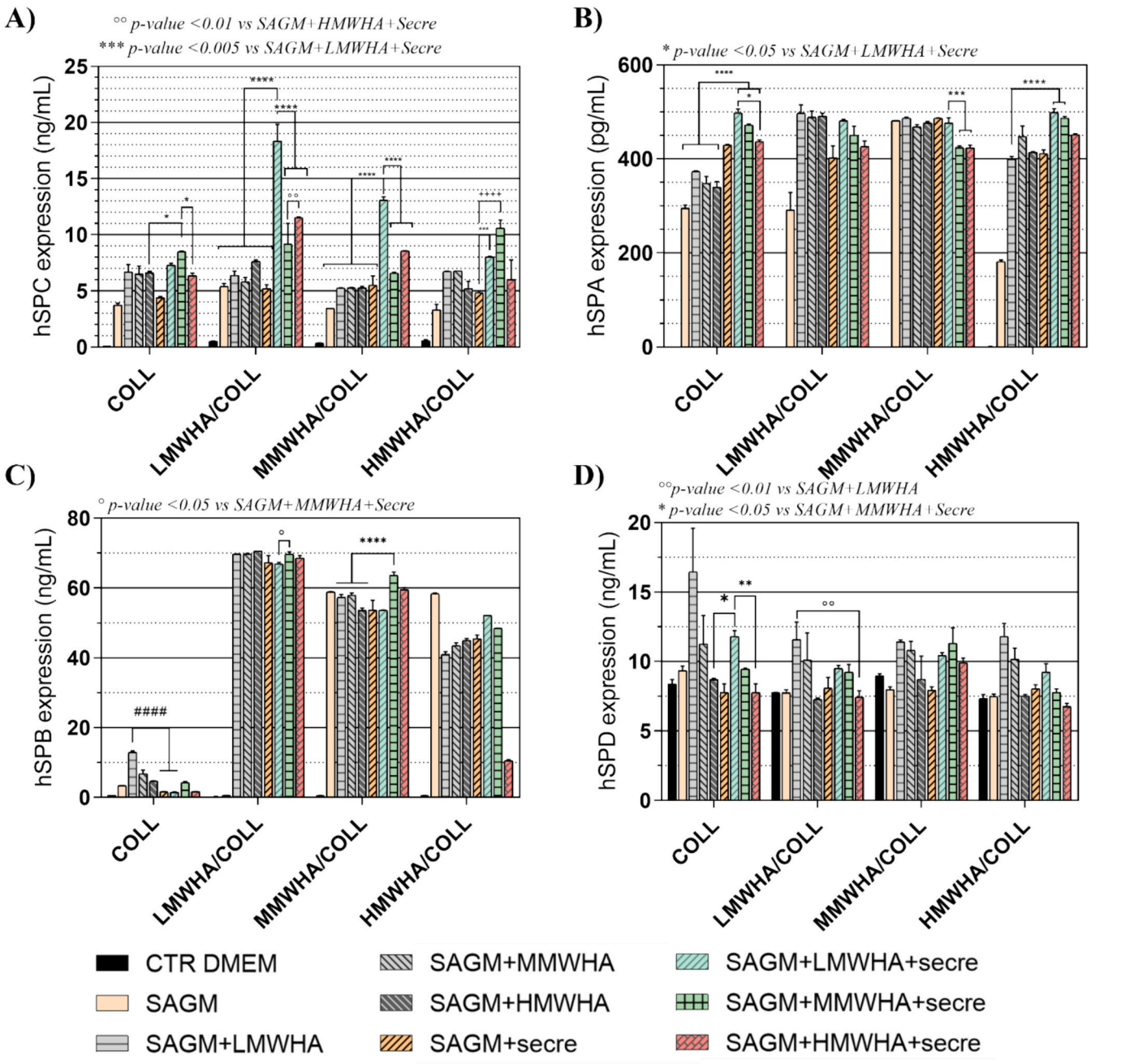

Fig. 7. Quantitative expression of SPC (A), SPA (B) and SPB (C) and SPD (D) performed by the ELISA kit test after the incubation of Secre, HA solutions, and HA/Secre blends implementing SAGM after 21 days of culture in a 3D biomimetic stem niche composed of COLL or COLL/HA gels at differentMWs. ****p-value<0.001.

of the secretome more tightly than the HMWHA.

3.6. Alveolar type II differentiation

In order to assess the occurrence of a bioactive cooperative effect of HA/Secre blends that could affect lung differentiation in 3D microenvironments, first, the qualitative differentiation of MSCs into ATII cells has been evaluated. The cells were stained with an SPC antibody, a specific pulmonary differentiation marker. The representative confocal images (Fig. 6) show the SPC antibody reactivity after 21 days in the cells embedded in the COLL, LMWHA/COLL, MMWHA/COLL, and HMWHA/COLL gels when incubated with the HA/Secre blends and HA solutions compared to MSCs maintained with only DMEM as controls. Positive expression of CD73 (red), a specific stemness marker, has been detected at day 0 and after 21 days of incubation, indicating the presence of undifferentiated cells only in the samples with control DMEM. Instead, green staining, indicating SPC positive expression, can be seen throughout the cytoplasm, with more intense staining observed in the perinuclear region of the samples incubated with HA/Secre blends, suggesting the presence of SPC in the Golgi/ER compartments.

Quantitative expression of SPC along with the other surfactant proteins SPA, SPB and SPD was evaluated by the ELISA kit (Fig. 7). The synthesis of SPC is a unique feature of ATII cells and is commonly used to identify these cells from other lung parenchymal cells [38]. The SPC expression (Fig. 7A), after the MSCs were seeded in the 3D microenvironment based on HA/COLL gels mimicking the lung niche, has proven to be higher in the presence of the HA/Secre blends compared to the use of only HA or Secre alone in solutions. Specifically, among the three blends analyzed, LMWHA/Secre has been shown to have an improved effect compared to MMWHA/Secre and HMWHA/Secre. In particular, in

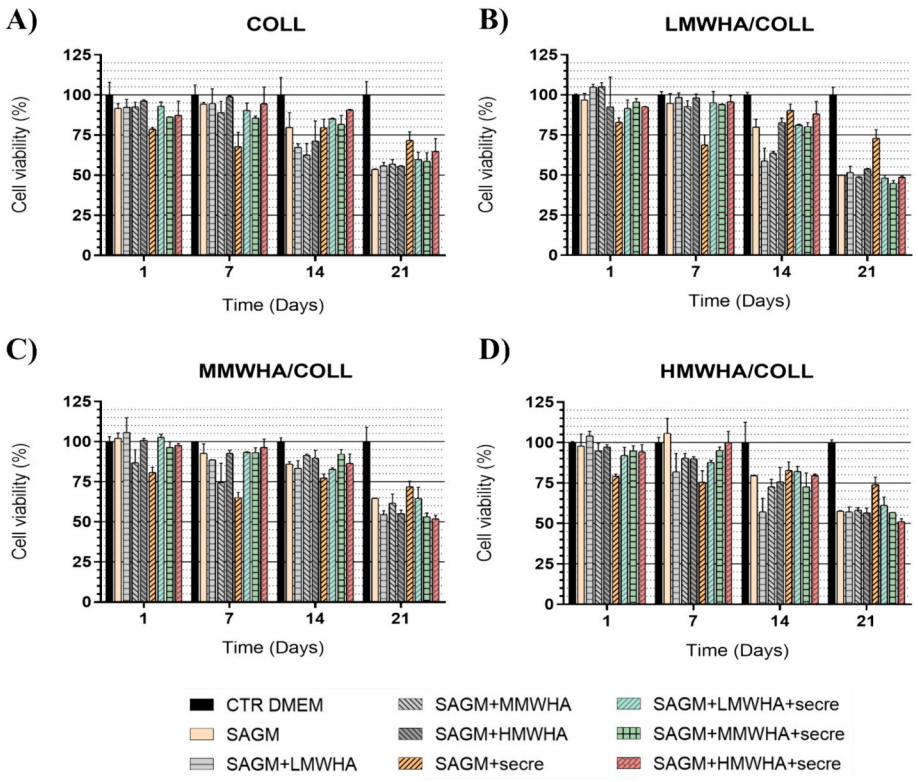

Fig. 8. Effect of Secre, HA solutions and Secre/HA blends implementing cell media on cell viability performed by the Alamar blue test in a 3D biomimetic stem niche composed of a COLL or COLL/HAgels. Viability percentage was reported as a function of time at 1, 7, 14 and 21 days of cell culture during the differentiation test. For each evaluated day of culture, all samples' viability is referred to as CTR DMEM as control on that specific day.

the HA/COLL 3D matrices, for the LMWHA/Secre blends, the SPC expression increases as the HA MWs in the matrices decrease, with values of around 19 ng ml^{-1} (LMWHA/COLL), of about 14 ng ml^{-1} (MMWHA/COLL) and of around 8 ng ml^{-1} (HMWHA/COLL). In any case, the values of LMWHA/Secre are always greater than the sum of the SPC expressions in presence of HA and Secre components alone in solution, indicating a bioactive cooperative effect of this biomaterial. The other blends showed a similar trend as the MWs varied but with lower values, with the exception of the HMWHA/COLL matrix, in which the LMWHA/Secre and MMWHA/Secre blends had comparable values. Furthermore, the exposure of HA/Secre blends in all HA/COLL gels mimicking 3D microenvironments showed SPC expression much higher compared to the 2D systems, as in our previous work, in which LMWHA and MMWHA plus secretome solution reached values of about 5 ng ml^{-1}. These results point out the importance of using 3D microenvironments that better resemble the complexity of in vivo conditions. The expression of the other surfactant proteins A, B and D (Fig. B, C, D) was found in the presence of the HA/Secre blends, further demonstrating pulmonary differentiation. These different amounts of expression could be explained by the diverse function of the SP, which is modulated according to cellular needs. The SPC is a specific lung marker with important functions that lead to a reduction in alveolar surface tension during respiration. SPB includes the structural transformation of the lamellar body to tubular myelin in the presence of Ca^{2+}, enhancing the reuptake of surfactant by endocytosis by ATII cells, and activating alveolar macrophages to facilitate surfactant clearance. Both SPA and SPD possess antimicrobial properties. SPA is chemotactic for macrophages and promotes bacterial phagocytosis [39]. These results demonstrate that the HA/Secre blends have an important effect on pulmonary differentiation compared to the use of HA or Secre alone in 3D microenvironments. Although the mechanism of interaction is unknown until now, what can be hypothesized is that HA interacts with the phospholipid bilayer of EVs like a coating, as happens for glycocalyx in nature. In fact, the glycocalyx, also known as the pericellular matrix, is a highly hydrated network of carbohydrates that protrudes and covers the membrane of various cells, epithelial and endothelial, and of many bacteria. The glycocalyx has been proposed to serve several important functions, including a critical role in cellular adhesion, signaling, and communication within the biological environment [40]. It can therefore be supposed that the HA layer interacting with the EVs can determine a consequent synergistic effect on lung differentiation, triggered by the presence of both components in solution. Moreover, we speculated that the interplay between HA and EVs in the blends can exert an improvement in biological functions as their physical-chemical interaction in solutions can increase the trafficking of the EVs by increasing the overall interaction of the EVs with the cell embedded in the 3D microenvironments. HA could act as a linker between EVs and cells in the 3D matrix, thus increasing adhesion and internalization into the target cell, increasing the overall biological potency of EVs. This could be in part explained since the hUCMSCs are known to express the CD44 receptor [41,42], and HA possesses a selective tropism for this receptor [43]. Furthermore, in light of this hypothesis, the interplay of the two components in solution can influence their biological functions depending on different HA MW. Indeed, it is known that a single HA chain contains multiple CD44 binding sites; thus, to interact with several CD44 receptors simultaneously on the cell membrane, the HA chain has to undergo conformational changes [44]. Thus, the possible HA conformations on the cell surface depend on the length and flexibility of its chain. High MW HA can assume several arrangements as large coils, resulting in a lower probability of sustaining stable bonds with CD44 receptor clusters on the cell surface [45]. In accordance with our data, the differentiation ability decreases when HA MW in solution increases, overall decreasing the bridging effect between EVs and cell membranes.

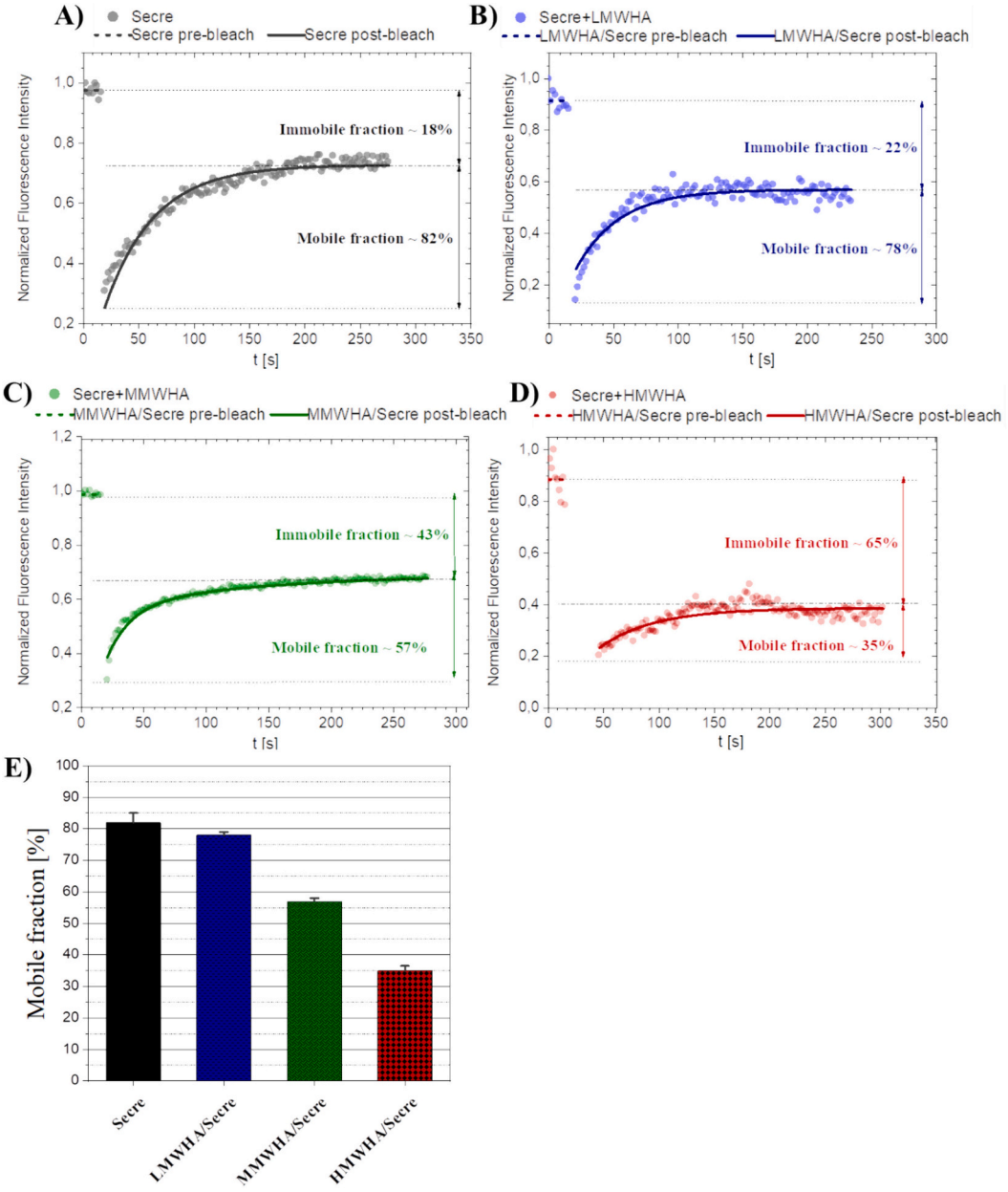

Fig. 9. Fluorescence recovery after photobleaching (FRAP) analysis on Secre (A) and HA/Secre blends for LMWHA (B), MMWHA (C) and HMWHA (D). Representative plots of normalized fluorescence intensity during and after photo-bleaching, the dots represent the original data, the continuous line represents data fitting after photo-bleaching, and the short dashed line represents the data fitting before photo-bleaching. Effect of different MW HA chains on the mobile fraction of the MVs (E).

3.7. Cell viability

The cell viability test has been performed during the differentiation time, until 21 days of culture in 3D systems mimicking the physiological environments. As observed in Fig. 8, a viability percentage of around 100 % has been found in all 3D gels in the presence of the HA/Secre blends. After 14 and 21 days of cell culture, the cell viability was about 70 % and 60 %, respectively, indicating that the differentiation stimuli occurred. Indeed, the development of the differentiation signals in the cells inhibits cellular proliferation in favour of a state of quiescence [46]. However, the viabilities of cells incubated with HA/Secre blends are always higher than in the presence of HA solutions alone, suggesting that the bioactive combination of HA/Secre together can amplify viability even in more complex systems, such as 3D gels.

3.8. Fluorescence recovery after photobleaching (FRAP)

FRAP analysis has been used to assess the interplay of HA chains at different MWs and MVs (Fig. 9.). EVs, Nile-red stained in this case, are produced by the cells themselves, and it is known that they have a phospholipid bilayer with components similar to those of cell membranes. The plasma membrane is known to behave as a fluid mosaic in which the components are mobile and capable of establishing transient or semi-permanent interactions [47]. Representative plots of the samples' fluorescence recovery have been reported in Fig. 9A, B, C and D. The normalized fluorescence intensities, both before and after photobleaching, appear to be narrowly distributed, and the mobile fractions M_f of MVs can be highlighted after performing data fitting. Indeed, it can be seen in Fig. 9B, C and D that the HA shows a decreasing effect on the M_f of MVs, reducing the secretome M_f from 82 % to lower values when

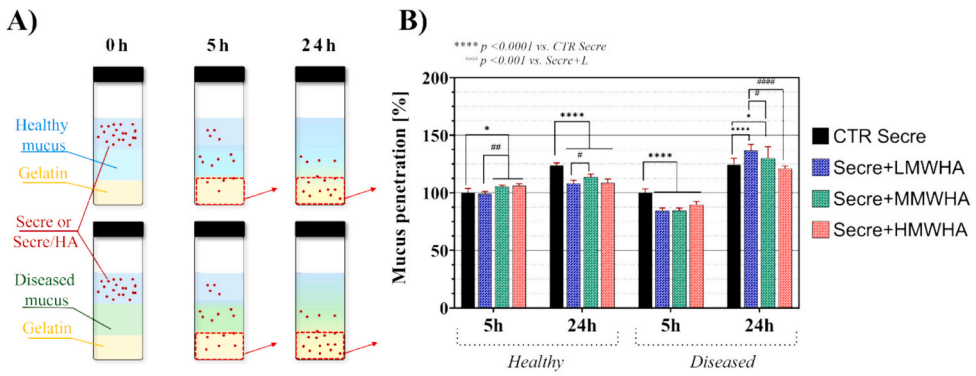

Fig. 10. In vitro assessment of mucus penetration. Schematic representation of the experiment (A). Outcome of the mucus penetration assay after 5 and 24 h on HM and DM. Data were obtained by normalization of fluorescence emission spectroscopy on Nile-red stained MVs compared to Secre control for HM and DM.

HA MWs increase. As a matter of fact, the interaction with LMWHA (Fig. 9B) brings a value of M_f equal to 78 %, decreasing to 57 % and 35 % for MMWHA (Fig. 9C) and HMWHA (Fig. 9D) respectively, as shown by the histogram in Fig. 9E. Thus, the FRAP analysis corroborated the general hypothesis of an interaction between the polysaccharide chains and the EVs. The fluidity of the cell membrane is essential for its functioning; a membrane too rigid would not allow mobility, and a membrane that is too fluid would lack mechanical support, and the components could not be oriented [48]. Data suggest that with increasing HA MWs, M_f % of the MVs decreased. These data are in accordance with the trend of the biological differentiation data, in which the differentiation power decreases as the MWs HA increases. The HA chains on EVs could act similarly to glycocalyx in transmitting physical forces to the cytoskeleton of cells to improve their fusion ability with the cell membranes. The presence of HMWHA leads to an increase in the immobile fraction percentage; on the contrary, in the presence of LMWHA and MMWHA the mobile fraction percentage appears to be higher. These findings could influence the interaction of EVs on the cell surface. Purportedly, the HMWHA in the blend can inhibit the exposure of EV functional groups, influencing the interaction with the cell surface. Indeed, by its nature, HMW species may form more intramolecular interactions arranging themselves in random coils with inaccessible potential interaction sites on the cell surface [49]. While LMWHA and MMWHA, forming more intermolecular interactions, have a more open conformation that exposes the carboxylate units to the phospholipids, allowing the CD44 binding [50].

3.9. *In vitro assessment of mucus penetration*

The ability of HA/Secre blends to cross the mucus layer is critical to achieve efficient delivery in the lungs. In order to perform a preliminary study on the effect of HA/Secre blends on mucus penetration, fluorescent Secre and HA/Secre blends were placed on a thick layer of HM and DM on a gelatine substrate (Fig. 10A). In Fig. 10B the quantitative evaluation of the mucus penetration by Secre alone as a control and HA/Secre in different blends is reported. In particular, after 5 h of incubation, the LMWHA/Secre penetrated the HM layer slightly less than the Secre control. Instead, MMWHA/Secre and HMWHA/Secre showed a significant penetration compared to Secre ($p < 0.05$) and a very significant ($p < 0.01$) effect compared to the LMWHA/Secre blend. Even though a slight level of significance is preserved with MMWHA/Secre, after 24 h of incubation, the trend is inverted since Secre penetrates the HM layer significantly more than HA/Secre blends. The DM, instead, shows some apparently counterintuitive results, since after 5 h of incubation, Secre control depicts a highly significant ($p < 0.0001$) penetration when compared to HA/Secre blends. This trend is totally inverted after 24 h incubation, since LMWHA/Secre shows the best effect on DM penetration, with the highest significance ($p < 0.0001$) when compared to Secre control and HMWHA/Secre blend. Still, a slight significance ($p < 0.05$) is visible comparing the penetration of LMWHA/Secre and MMWHA/Secre, suggesting the first as the best blend to penetrate DM. This could be explained by the establishment of repulsive forces as a consequence of the formation of polyanionic domains of HA and mucin chains, leading to a reduction of mucin adsorption and an enhancement of permeability [51].

4. Conclusions

Previous studies showed the biological action of the HA/Secre blends in promoting lung regeneration in 2D cell culture systems, far removed from the real physiology of tissues, without focusing on the interplay of the two components in the blends. In this study, we successfully investigated the effect of physicochemical properties of HA/Secre blends with different MWs HA (L, M and H) by means of SEM/TEM, DLS, FTIR and FRAP analysis. Morphological characterization and the physical-chemical analyses have shown an interplay between the HA and the EVs of the secretome. In particular, these results suggest that the HA MW exerts an important influence on the physical-chemical properties of the HA/Secre blends, since the HA chains would seem to cover the EV population depending on the increase of their MW. Furthermore, our findings demonstrated for the first time that HA/Secre blends are able to induce pulmonary differentiation of MSCs and to support cellular viability in 3D matrices mimicking the lung microenvironments that better resemble in vivo conditions. The differentiation power of the HA/Secre blends increases as the HA MWs decrease, and this trend is in agreement with the mobility percentage data of EVs in solution with the different HA MWs. This may suggest that highly hydrated carbohydrates, such as HA, that protrude and coat the membranes of EVs may influence the transmission of other physical forces that act on the cytoskeleton of cells, influencing their biological function. Especially in 3D systems, where the forces of the matrix in which the cells are embedded also act. Finally, the ability of HA/Secre blends to cross the mucus layer, essential to achieve efficient delivery in the lungs, has been assessed. In accordance with the trend of differentiation study, it was found to be higher after 24 h in a diseased mucus model for the LMWHA/Secre blends, indicating also in this case that, despite their interplay, other repulsive forces in the 3D mucus matrix affect the behaviour of the blends. In this direction, further studies are required in order to elucidate the specific type of interaction, e.g., purely electrostatic or receptor-mediated, that occurs between the two components in the blends. Furthermore, a study aimed at understanding the uptake of EVs in target cells would be useful in order to delve deeper into the importance of the use of HA/Secre blends both in 2D and 3D culture systems. These findings can expand knowledge and allow the optimization of the rational design of future devices, including HA and secretome useful in lung regeneration fields.

CRediT authorship contribution statement

Francesca Della Sala: Writing – review & editing, Writing – original draft, Investigation, Data curation, Conceptualization. **Gennaro Longobardo:** Writing – original draft, Investigation, Data curation. **Mario di Gennaro:** Writing – original draft, Investigation, Data curation. **Francesco Messina:** Visualization. **Assunta Borzacchiello:** Writing – review & editing, Visualization, Supervision, Resources.

Declaration of competing interest

The authors declare that they have no known competing financial interests or personal relationships that could have appeared to influence the work reported in this paper.

Appendix A. Supplementary data

Supplementary data to this article can be found online at https://doi.org/10.1016/j.ijbiomac.2024.133793.

References

[1] M. Rojas, A.L. Mora, M. Kapetanaki, N. Weathington, M. Gladwin, O. Eickelberg, Aging and lung disease. Clinical impact and cellular and molecular pathways, Ann. Am. Thorac. Soc. 12 (12) (2015) S222–S227, https://doi.org/10.1513/AnnalsATS.201508-484PL.

[2] T.H.G. Phan, P. Paliogiannis, G.K. Nasrallah, R. Giordo, A.H. Eid, A.G. Fois, A. Zinellu, A.A. Mangoni, G. Pintus, Emerging cellular and molecular determinants of idiopathic pulmonary fibrosis, Cell. Mol. Life Sci. 78 (2021) 2031–2057, https://doi.org/10.1007/s00018-020-03693-7.

[3] S.D. Nathan, J.A. Barbera, S.P. Gaine, S. Harari, F.J. Martinez, H. Olschewski, K. M. Olsson, A.J. Peacock, J. Pepke-Zaba, S. Provencher, Pulmonary hypertension in chronic lung disease and hypoxia, Eur. Respir. J. 53 (1) (2019), https://doi.org/10.1183/13993003.01914-2018.

[4] F.M. Franssen, P. Alter, N. Bar, B.J. Benedikter, S. Iurato, D. Maier, M. Maxheim, F. K. Roessler, M.A. Spruit, C.F. Vogelmeier, Personalized medicine for patients with COPD: where are we? Int. J. Chron. Obstruct. Pulmon. Dis. (2019) 1465–1484, https://doi.org/10.2147/COPD.S175706.

[5] F.F. Cruz, P.R.M. Rocco, The potential of mesenchymal stem cell therapy for chronic lung disease, Expert Rev. Respir. Med. 14 (1) (2020) 31–39, https://doi.org/10.1080/17476348.2020.1679628.

[6] S. El Andaloussi, I. Mäger, X.O. Breakefield, M.J. Wood, Extracellular vesicles: biology and emerging therapeutic opportunities, Nat. Rev. Drug Discov. 12 (5) (2013) 347–357, https://doi.org/10.1038/nrd3978.

[7] S. Öztürk, A.E. Elçin, Y.M. Elçin, Functions of mesenchymal stem cells in cardiac repair, Cell Biology and Translational Medicine, Volume 11: Stem Cell Therapy-Potential and Challenges, Springer2020, pp. 39–50.

[8] F.J. Vizoso, N. Eiro, S. Cid, J. Schneider, R. Perez-Fernandez, Mesenchymal stem cell secretome: toward cell-free therapeutic strategies in regenerative medicine, Int. J. Mol. Sci. 18 (9) (2017) 1852, https://doi.org/10.3390/ijms18091852.

[9] S.K. Kapur, A.J. Katz, Review of the adipose derived stem cell secretome, Biochimie 95 (12) (2013) 2222–2228, https://doi.org/10.1016/j.biochi.2013.06.001.

[10] M. Arifka, G. Wilar, K.M. Elamin, N. Wathoni, Polymeric hydrogels as mesenchymal stem cell Secretome delivery system in biomedical applications, Polymers 14 (6) (2022) 1218, https://doi.org/10.3390/polym14061218.

[11] T. Später, M. Assunção, K.K. Lit, G. Gong, X. Wang, Y.-Y. Chen, Y. Rao, Y. Li, C.H. K. Yiu, M.W. Laschke, Engineering microparticles based on solidified stem cell secretome with an augmented pro-angiogenic factor portfolio for therapeutic angiogenesis, Bioact. Mater. 17 (2022) 526–541, https://doi.org/10.1016/j.bioactmat.2022.03.015.

[12] M. Mohammadi, J.C. Luong, S.M. Rodriguez, R. Cao, A.E. Wheeler, H. Lau, S. Li, S. K. Shabestari, J.P. Chadarevian, M. Alexander, Controlled release of stem cell secretome attenuates inflammatory response against implanted biomaterials, Adv. Healthc. Mater. 9 (12) (2020) 1901874, https://doi.org/10.1002/adhm.201901874.

[13] K. Morimoto, K. Metsugi, H. Katsumata, K. Iwanaga, M. Kakemi, Effects of low-viscosity sodium hyaluronate preparation on the pulmonary absorption of rh-insulin in rats, Drug Dev. Ind. Pharm. 27 (4) (2001) 365–371, https://doi.org/10.1081/DDC-100103737.

[14] P. Makvandi, F. Della Sala, M. di Gennaro, N. Solimando, M. Pagliuca, A. Borzacchiello, A hyaluronic acid-based formulation with simultaneous local drug delivery and antioxidant ability for active viscosupplementation, ACS Omega 7 (12) (2022) 10039–10048, https://doi.org/10.1021/acsomega.1c05622.

[15] F. Della Sala, M. di Gennaro, G. Lista, F. Messina, L. Ambrosio, A. Borzacchiello, Effect of hyaluronic acid on the differentiation of mesenchymal stem cells into mature type II Pneumocytes, Polymers 13 (17) (2021) 2928, https://doi.org/10.3390/polym13172928.

[16] F. Della Sala, M. di Gennaro, G. Lista, F. Messina, T. Valente, A. Borzacchiello, Effect of composition of lung biomimetic niche on the mesenchymal stem cell differentiation toward alveolar type II Pneumocytes, Macromol. Biosci. 23 (6) (2023) 2300035, https://doi.org/10.1002/mabi.202300035.

[17] F. Della Sala, G. Longobardo, G. Lista, F. Messina, A. Borzacchiello, Effect of hyaluronic acid and mesenchymal stem cells Secretome combination in promoting alveolar regeneration, Int. J. Mol. Sci. 24 (4) (2023) 3642, https://doi.org/10.3390/ijms24043642.

[18] C. Jensen, Y. Teng, Is it time to start transitioning from 2D to 3D cell culture? Front. Mol. Biosci. 7 (2020) 33, https://doi.org/10.3389/fmolb.2020.00033.

[19] T. Volckaert, S. De Langhe, Lung epithelial stem cells and their niches: Fgf10 takes center stage, Fibrogenesis Tissue Repair 7 (2014) 1–15, https://doi.org/10.1186/1755-1536-7-8.

[20] E. Bari, S. Perteghella, D. Di Silvestre, M. Sorlini, L. Catenacci, M. Sorrenti, G. Marrubini, R. Rossi, G. Tripodo, P. Mauri, Pilot production of mesenchymal stem/stromal freeze-dried secretome for cell-free regenerative nanomedicine: a validated GMP-compliant process, Cells 7 (11) (2018) 190, https://doi.org/10.3390/cells7110190.

[21] B. Varghese, Z. Ling, X. Ren, Reconstructing the pulmonary niche with stem cells: a lung story, Stem Cell Res Ther 13 (1) (2022) 161, https://doi.org/10.1186/s13287-022-02830-2.

[22] F. Della Sala, B.M. Malle, L. Ambrosio, A. Borzacchiello, Fermentation-derived albumin-based hydrogels for tissue adhesion applications, Polymers 15 (11) (2023) 2530, https://doi.org/10.3390/polym15112530.

[23] J. Wu, T. Zhai, J. Sun, Q. Yu, Y. Feng, R. Li, H. Wang, Q. Ouyang, T. Yang, Q. Zhan, Mucus-permeable polymyxin B-hyaluronic acid/poly (lactic-co-glycolic acid) nanoparticle platform for the nebulized treatment of lung infections, J. Colloid Interface Sci. 624 (2022) 307–319, https://doi.org/10.1016/j.jcis.2022.05.121.

[24] W.W. Graessley, Polymer chain dimensions and the dependence of viscoelastic properties on concentration, molecular weight and solvent power, Polymer 21 (3) (1980) 258–262, https://doi.org/10.1016/0032-3861(80)90266-9.

[25] X. Chen, Y. Zhang, H. Wang, S.-W. Wang, S. Liang, R.H. Colby, Solution rheology of cellulose in 1-butyl-3-methyl imidazolium chloride, J. Rheol. 55 (3) (2011) 485–494, https://doi.org/10.1122/1.3553032.

[26] E. Zhang, X. Dai, Z. Dong, X. Qiu, X. Ji, Critical concentration and scaling exponents of one soluble polyimide—from dilute to semidilute entangled solutions, Polymer 84 (2016) 275–285, https://doi.org/10.1016/j.polymer.2016.01.001.

[27] A. El Aferni, M. Guettari, M. Kamli, T. Tajouri, A. Ponton, A structural study of a polymer-surfactant system in dilute and entangled regime: effect of high concentrations of surfactant and polymer molecular weight, J. Mol. Struct. 1199 (2020) 127052, https://doi.org/10.1016/j.molstruc.2019.127052.

[28] C. Jaudoin, M.M. Gehrke, I. Grillo, F. Cousin, M. Ouldali, A.-A. Arteni, E. Ferrary, F. Siepmann, J. Siepmann, F. Simelière, Release of liposomes from hyaluronic acid-based hybrid systems: effects of liposome surface and size, Int. J. Pharm. 648 (2023) 123560, https://doi.org/10.1016/j.ijpharm.2023.123560.

[29] N. Kozer, Y.Y. Kuttner, G. Haran, G. Schreiber, Protein-protein association in polymer solutions: from dilute to semidilute to concentrated, Biophys. J. 92 (6) (2007) 2139–2149, https://doi.org/10.1529/biophysj.106.097717.

[30] N. El Kechai, S. Geiger, A. Fallacara, I.C. Infante, V. Nicolas, E. Ferrary, N. Huang, A. Bochot, F. Agnely, Mixtures of hyaluronic acid and liposomes for drug delivery: phase behavior, microstructure and mobility of liposomes, Int. J. Pharm. 523 (1) (2017) 246–259, https://doi.org/10.1016/j.ijpharm.2017.03.029.

[31] M. Salazar, H. Srivastav, A. Srivastava, S. Srivastava, A user-friendly graphical user Interface for dynamic light scattering data analysis, Soft Matter 19 (2023) 6535–6544, https://doi.org/10.1039/D3SM00469D.

[32] A.e. Scotti, W. Liu, J. Hyatt, E. Herman, H. Choi, J. Kim, L. Lyon, U. Gasser, A. Fernandez-Nieves, The CONTIN algorithm and its application to determine the size distribution of microgel suspensions, J. Chem. Phys. 142(23) (2015), doi:https://doi.org/10.1063/1.4921686.

[33] F. Rad, A.A. Pourfathollah, F. Yari, S. Mohammadi, M. Kheirandish, Microvesicles preparation from mesenchymal stem cells, Med. J. Islam Repub. Iran 30 (2016) 398.

[34] A. Dodero, R. Williams, S. Gagliardi, S. Vicini, M. Alloisio, M. Castellano, A micro-rheological and rheological study of biopolymers solutions: hyaluronic acid, Carbohydr. Polym. 203 (2019) 349–355, https://doi.org/10.1016/j.carbpol.2018.09.072.

[35] J. Mihály, R. Deák, I.C. Szigyártó, A. Bóta, T. Beke-Somfai, Z. Varga, Characterization of extracellular vesicles by IR spectroscopy: fast and simple classification based on amide and CH stretching vibrations, Biochim. Biophys. Acta Biomembr. 1859 (3) (2017) 459–466, https://doi.org/10.1016/j.bbamem.2016.12.005.

[36] V. Conti Nibali, C. Branca, U. Wanderlingh, G. D'Angelo, Intermolecular hydrogen-bond interactions in DPPE and DMPC phospholipid membranes revealed by far-infrared spectroscopy, Appl. Sci. 11 (21) (2021) 10038, https://doi.org/10.3390/app112110038.

[37] M. Dovedytis, Z.J. Liu, S. Bartlett, Hyaluronic acid and its biomedical applications: a review, Eng. Regen. 1 (2020) 102–113, https://doi.org/10.1016/j.engreg.2020.10.001.

[38] D. Wang, D.L. Haviland, A.R. Burns, E. Zsigmond, R.A. Wetsel, A pure population of lung alveolar epithelial type II cells derived from human embryonic stem cells, Proc. Natl. Acad. Sci. 104 (11) (2007) 4449–4454, https://doi.org/10.1073/pnas.0700052104.

[39] N.V. Bhagavan, CHAPTER 19 - lipids II: Phospholipids, glycosphingolipids, and cholesterol, in: N.V. Bhagavan (Ed.), Medical Biochemistry (Fourth Edition), Academic Press, San Diego, 2002, pp. 401–427.

[40] R. Uchimido, E.P. Schmidt, N.I. Shapiro, The glycocalyx: a novel diagnostic and therapeutic target in sepsis, Crit. Care 23 (1) (2019) 16, https://doi.org/10.1186/s13054-018-2292-6.

[41] H.S. Wang, S.C. Hung, S.T. Peng, C.C. Huang, H.M. Wei, Y.J. Guo, Y.S. Fu, M.C. Lai, C.C. Chen, Mesenchymal stem cells in the Wharton's jelly of the human umbilical cord, Stem Cells 22 (7) (2004) 1330–1337, https://doi.org/10.1634/stemcells.2004-0013.

[42] H. Ali, M.K. Al-Yatama, M. Abu-Farha, K. Behbehani, A. Al Madhoun, Multi-lineage differentiation of human umbilical cord Wharton's jelly mesenchymal stromal cells mediates changes in the expression profile of stemness markers, PloS One 10 (4) (2015) e0122465, https://doi.org/10.1371/journal.pone.0122465.

[43] G. Agarwal, S. Agiwal, A. Srivastava, Hyaluronic acid containing scaffolds ameliorate stem cell function for tissue repair and regeneration, Int. J. Biol. Macromol. 165 (2020) 388–401, https://doi.org/10.1016/j.ijbiomac.2020.09.107.

[44] P.M. Wolny, S. Banerji, C. Gounou, A.R. Brisson, A.J. Day, D.G. Jackson, R. P. Richter, Analysis of CD44-hyaluronan interactions in an artificial membrane system: insights into the distinct binding properties of high and low molecular weight hyaluronan, J. Biol. Chem. 285 (39) (2010) 30170–30180, https://doi.org/10.1074/jbc.M110.137562.

[45] S. Banerji, A.J. Wright, M. Noble, D.J. Mahoney, I.D. Campbell, A.J. Day, D. G. Jackson, Structures of the Cd44–hyaluronan complex provide insight into a fundamental carbohydrate-protein interaction, Nat. Struct. Mol. Biol. 14 (3) (2007) 234–239, https://doi.org/10.1038/nsmb1201.

[46] S. Ruijtenberg, S. van den Heuvel, Coordinating cell proliferation and differentiation: antagonism between cell cycle regulators and cell type-specific gene expression, Cell Cycle 15 (2) (2016) 196–212, https://doi.org/10.1080/15384101.2015.1120925.

[47] R. Yamaguchi, Y. Kanie, T. Kazamaki, O. Kanie, Y. Shimizu, Cellular uptake of liposome consisting mainly of glucocerebroside from the starfish Asterias amurensis into Caco-2 cells, Carbohydr. Res. 532 (2023) 108921, https://doi.org/10.1016/j.carres.2023.108921.

[48] A. NIGEL CHAFFEY, B., Johnson, A., Lewis, J., Raff, M., Roberts, K. and Walter, P. , Molecular Biology of the Cell. 4th edn., Annals of Botany,, Oxford University Press, 2003, p. 401.

[49] P. Bełdowski, S. Yuvan, A. Dėdinaitė, P.M. Claesson, T. Pöschel, Interactions of a short hyaluronan chain with a phospholipid membrane, Colloids Surf. B Biointerfaces 184 (2019) 110539, https://doi.org/10.1016/j.colsurfb.2019.110539.

[50] M. Herzog, L. Li, H.-J. Galla, R. Winter, Effect of hyaluronic acid on phospholipid model membranes, Colloids Surf. B Biointerfaces 173 (2019) 327–334, https://doi.org/10.1016/j.colsurfb.2018.10.006.

[51] K.B. Japiassu, F. Fay, A. Marengo, Y. Louaguenouni, C. Cailleau, S. Denis, D. Chapron, N. Tsapis, T.L. Nascimento, E.M. Lima, Interplay between mucus mobility and alveolar macrophage targeting of surface-modified liposomes, J. Control. Release 352 (2022) 15–24, https://doi.org/10.1016/j.jconrel.2022.10.006.